This article has been accepted for publication in IEEE Antennas and Wireless Propagation Letters. This is the author's version which has not been fully edited and content may change prior to final publication. Citation information: DOI 10.1109/LAWP.2026.3746048

Miniaturized Dual-Port Frequency-Isolated Implantable Antenna for Self-Duplexing Capsule Endoscopy

Izhar Khan, Sarosh Ahmad, *Member, IEEE*, Syed Manaf Ali Shah, Idris Saadu Idris, Harris Sarfraz, Xue Jun Li, *Senior Member, IEEE* and Tayeb A. Denidni, *Fellow, IEEE*

***Abstract*—This letter presents a miniaturized dual-port self-duplexing implantable antenna for wireless capsule endoscopy (WCE) applications. The proposed antenna provides two independently excited frequency-isolated channels centered at 0.868 (Port 2) and 1.41 GHz (Port 1), intended to support self-duplexing WCE telemetry without an external antenna duplexing network. The antenna occupies a compact volume of only $\pi \times (2.5)^2 \times 0.26 = 5.11$ mm^3 and employs a planar stub-loaded configuration with a full ground plane. The two ports provide isolation levels of approximately 22 and 35 dB at 0.868 and 1.41 GHz, respectively, while maintaining impedance bandwidths of approximately 120 and 110 MHz. The corresponding peak realized gains are -38 and -34.9 dBi. The specific absorption rate (SAR) performance is investigated in a human-body environment to assess the allowable excitation levels for safe implant operation. A prototype of the proposed antenna is fabricated and experimentally characterized in tissue-representative media, with the measured response showing reasonable agreement with the numerical results. The compact footprint, independent frequency-selective ports, high interport isolation, and experimentally verified operation make the proposed antenna a suitable candidate for bidirectional telemetry in WCE systems.**

***Index Terms*—Biomedical telemetry, frequency isolation, implantable antenna, self-duplexing, wireless capsule endoscopy (WCE).**

I. Introduction

IMPLANTABLE biomedical telemetry enables continuous physiological monitoring and wireless communication with devices located inside the human body, including the gastrointestinal tract and other internal organs [1]. These systems can collect information from regions that are difficult to monitor using conventional diagnostic methods and transmit the acquired data to an external unit [2], [3]. In such systems, the antenna plays a central role, as its size and electromagnetic performance directly affect device integration and communication reliability [4], [5]. Therefore, compact implantable antennas capable of supporting reliable wireless links within a limited device volume are highly desirable.

To support multiple wireless functions within a small footprint, several dual-band and multiband implantable antennas have been reported [6]. Miniaturization is commonly achieved using high-permittivity substrates, slots, extended current paths, loading stubs, and modified or defected ground structures (DGSs) [7]. However, achieving multiple resonances while preserving compact size, suitable impedance matching, and low inter-port coupling remains challenging [8]. For example, the triple-band antenna in [9] occupies 285.75 mm^3, while the design in [10] requires an external multiplexing network.

I. Khan, S. Ahmad, and S. M. A. Shah are the co-first authors. (Corresponding author: Sarosh Ahmad).
I. Khan, H. Sarfraz, X.J. Li are with the Department of Electrical and Electronic Engineering at Auckland University of Technology (AUT), Auckland, New Zealand. (e-mail: izharqazi839@gmail.com; harris.sarfraz@autuni.ac.nz; xuejun.li@aut.ac.nz).
S. Ahmad and T. A. Denidni are with the Énergie Matériaux Télécommunications Research Centre (EMT), Institut National de la Recherche Scientifique (INRS), Montréal, QC H5A 1K6, Canada. (e-mail: sarosh.ahmad@inrs.ca; tayeb.denidni@inrs.ca).
S. M. A. Shah is with the Department of Electrical and Computer Engineering, COMSATS University Islamabad, Abbottabad 22060, Pakistan. (e-mail: smas.cuiatd@gmail.com).
I.S. Idris is with the Pan African University Institute for Basic Sciences, Technology and Innovation (PAUSTI), Hosted at Jomo Kenyatta University of Agriculture and Technology (JKUAT), Nairobi, Kenya. (e-mail: idris.saadu@students.jkuat.ac.ke).

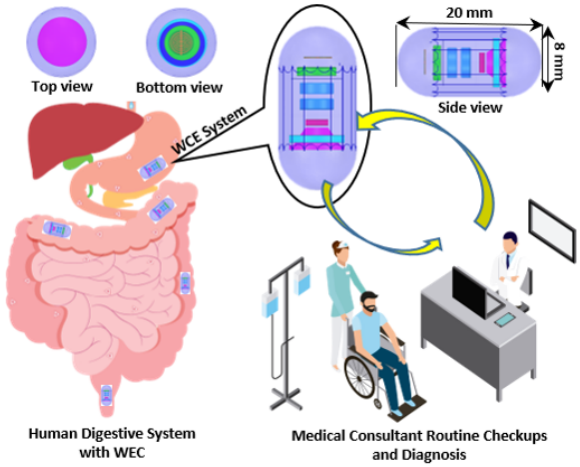


Fig. 1. Conceptual WCE system showing the proposed 0.868-GHz uplink and 1.41-GHz downlink channels and the in-body implementation of the dual-port antenna.

Another triple-band configuration in [11] occupies 64 mm^3. These studies highlight the continuing tradeoff among antenna size, multiband operation, and RF front-end complexity in implantable systems.

Multiband operation does not inherently provide separate transmit and receive channels, since multiple resonances may still share the same antenna port. In such cases, additional filtering or multiplexing circuitry is required to separate the communication paths, increasing the RF front-end complexity and occupied volume [12]. Self-duplexing antennas provide an alternative by using frequency-selective ports for independent transmission and reception without an external duplexing network [13], [14]. Several implantable self-duplexing configurations have been reported for this purpose [15]–[19]. However, many rely on shorting vias, slots, modified ground structures, or relatively complex radiator geometries to achieve miniaturization and adequate inter-port isolation. Developing a highly compact self-duplexing antenna with a simple structure, independently controlled channels, and strong port isolation therefore remains challenging for space-constrained implantable systems.

Recent implantable antennas have explored multiband and differential configurations [20]– [23]; however, these designs rely on multiresonant, differential, or fractal structures and do not provide two independently frequency-selective ports for separate transmit and receive channels. In contrast, the proposed antenna provides independent frequency-isolated dual-port operation without external antenna duplexing circuitry or differential feeding while maintaining a compact and simple configuration with high interport isolation. A detailed comparison with recent implantable antennas is provided in Table I.

Motivated by these limitations, this work presents a miniaturized dual-port frequency-isolated antenna for wireless capsule endoscopy (WCE). The 0.868-GHz channel is assigned to the implant-to-external-device uplink, where sub-GHz operation provides comparatively lower propagation loss, whereas the 1.41-GHz channel provides a spectrally separated downlink for control, synchronization, and auxiliary telemetry. The two independently controlled ports therefore provide frequency-domain separation between the uplink and down-

Authorized licensed use limited to: Auckland University of Technology. Downloaded on November 09,2026 at 22:06:40 UTC from IEEE Xplore. Restrictions apply.
© 2026 IEEE. All rights reserved, including rights for text and data mining and training of artificial intelligence and similar technologies. Personal use is permitted, but republication/redistribution requires IEEE permission. See https://www.ieee.org/publications/rights/index.html for more information.

This article has been accepted for publication in IEEE Antennas and Wireless Propagation Letters. This is the author's version which has not been fully edited and content may change prior to final publication. Citation information: DOI 10.1109/LAWP.2026.3746048

TABLE I
BENCHMARKING OF THE PROPOSED SELF-DUPLEXING ANTENNA AGAINST RECENT IMPLANTABLE DESIGNS.

Ref.	Dimensions (mm^3)	Freq. (GHz)	10-g SAR (W/kg)	Gain (dBi)	Isolation (dB)	BW (MHz)	Implant Location	Ports	STAR
[11]	$32 \times 10 \times 0.025$	0.402/0.9/2.4	316/358/247*	$-29.7/-28.7/-20.8$	–	236/10.4/55.4	Intestine	1	×
[12]	$17.25 \times 8 \times 0.635$	0.433/0.915	179.7/160.7	$-28.2/-24.5$	–	138/199	Mouth	1	×
[13]	$7.13 \times 8.9 \times 0.13$	0.915/1.42	440.2/408.8*	$-18.94/-17.06$	> 25	103/150*	Head	2	✓
[14]	$8 \times 8 \times 0.13$	0.915/1.3	297.3/1.08	$-19.3/-17.7$	> 25	172/200*	Head	2	✓
[15]	$9.6 \times 9.6 \times 0.26$	0.915/1.47	331.4/241.1*	$-26.8/-18.8$	> 20	90/108	Intestine	2	✓
[16]	$\pi(3.2)^2 \times 0.254$	1.8/2.4	18.9/20.6	$-24.7/-23.9$	> 25	360/390*	Stomach	2	✓
[17]	$10 \times 10 \times 0.1$	1.57	44.8	-20.93	> 20	495	Head	2	✓
[18]	$\pi(2.7)^2 \times 0.254$	2.45	36.8	$-20.2/-20.3$	> 25	210	Stomach	2	✓
[19]	$\pi(5.1)^2 \times 0.254$	0.433/0.915	91.7/96.4	$-36/-25$	> 20	151/273	Stomach	2	✓
[20]	$15 \times 12 \times 0.25$	0.902/1.4/1.9	36.2/38.2/24.1	$-25.86/-28.86/-33.02$	–	60/80/100	Stomach	1	×
[21]	$\pi(8)^2 \times 26$	0.402/1.5/2.45	–	$-35.6/-32.3/-31.4$	–	30/50/80	Stomach/Heart	1	×
[22]	$13 \times 13 \times 0.635$	0.915/2.45	–	$-30.3/-21.2$	–	40/140	Scalp/Heart	2	×
[23]	$9.5 \times 9.5 \times 0.635$	0.402/2.45	47.9/45.5	$-28.1/-31.3$	< 15	30/80	Arm	2	×
This Work	$\pi(2.5)^2 \times 0.26$	0.868/1.41	74.8/99.4	$-38/-34.9$	22/35	120/110	Stomach	2	✓

STAR: Simultaneous Transmit-and-Receive capability through independent Tx/Rx channels; * denotes 1-g SAR.

link paths without requiring an external antenna duplexing network. Despite its compact volume of only $\pi \times (2.5)^2 \times 0.26 = 5.11$ mm^3, the antenna achieves port isolation of approximately 22 and 35 dB at the two operating frequencies, respectively. The design further combines a full-ground configuration with a simple planar topology while providing SAR-compliant operation and nearly omnidirectional radiation characteristics. These features provide a compact frequency-isolated dual-port solution intended for bidirectional self-duplexing WCE telemetry.

II. ANTENNA CONFIGURATION AND DESIGN METHODOLOGY

The conceptual implementation of the proposed self-duplexing antenna within a wireless capsule endoscopy (WCE) system is illustrated in Fig. 1. The antenna is integrated with the PCB, battery, image sensor, LEDs, and associated electronics inside a 3-D-printed polylactic acid (PLA) capsule shell. PLA ($\varepsilon_r = 2.8$) is selected owing to its biocompatibility, biodegradability, and suitability for 3-D printing. The complete capsule assembly is incorporated into the electromagnetic model and evaluated in both homogeneous and heterogeneous gastrointestinal environments. For experimental validation, the fabricated PLA-enclosed capsule is characterized in tissue-representative media. In the proposed system architecture, Port 2 (0.868 GHz) is assigned to the capsule-to-external-device uplink, whereas Port 1 (1.41 GHz) supports the external-device-to-capsule downlink; the antenna remains reciprocal and the channel assignment is defined at the transceiver level.

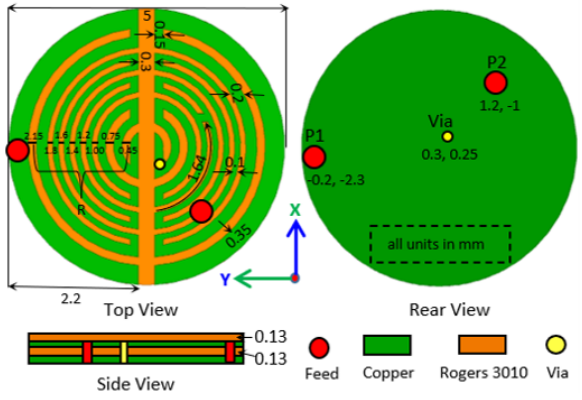


Fig. 2. Geometry and dimensional details of the proposed dual-port self-duplexing antenna.

A. Frequency-Isolated Dual-Port Antenna Configuration

The geometry of the proposed self-duplexing implantable antenna is illustrated in Fig. 2. The antenna is realized on a 0.26-mm-thick Rogers RO3010 substrate ($\varepsilon_r = 10.2$, $\tan\delta = 0.0022$), whose high permittivity facilitates substantial miniaturization. Two independently excited radiating sections are formed using compact loading stubs and slots, while a full ground plane is employed on the opposite side. Each port is excited through a 50-Ω coaxial probe with a radius of 0.15 mm.

With an overall radius of 2.5 mm and a total dielectric thickness of 0.26 mm, the antenna occupies a compact volume of $\pi(2.5)^2(0.26) = 5.11$ mm^3. The inter-element spacing and loading paths are jointly optimized to establish two frequency-selective resonances with limited current overlap, thereby suppressing mutual coupling between the ports. This compact arrangement enables independent frequency-selective operation with high interport isolation, making the antenna suitable for space-constrained wireless capsule endoscopy systems.

B. Progressive Miniaturization and Resonance Control

The stepwise development of the two frequency-selective radiators and their corresponding reflection coefficients is presented in Fig. 3. Starting from simple semicircular radiators, successive loading elements are introduced to extend the effective surface-current paths and independently shift the two resonances toward the desired operating bands.

Step I: The initial semicircular configurations exhibit resonances at approximately 1.85 and 2.75 GHz, as observed in Figs. 3(a) and 3(b), respectively. Owing to the electrically short current paths, both resonances remain considerably above the targeted frequencies.

Step II: Introducing the first set of curved loading sections increases the effective electrical lengths without enlarging the antenna footprint. Consequently, the resonances shift downward to approximately 1.70 GHz in Fig. 3(a) and 1.44 GHz in Fig. 3(b), with improved impedance matching.

Step III: Further extension of the concentric loading paths provides the required miniaturization and resonance control. The final configurations resonate at approximately 0.86 and 1.41 GHz, respectively, while exhibiting strong impedance matching. This progressive evolution demonstrates that the two radiators can be independently tailored through their effective current paths, enabling compact dual-frequency operation for the proposed self-duplexing WCE antenna.

The effect of the metallic via is illustrated in Fig. 3(c), where the via-loaded configuration preserves the intended resonances near

Authorized licensed use limited to: Auckland University of Technology. Downloaded on November 09,2026 at 22:06:40 UTC from IEEE Xplore. Restrictions apply.
© 2026 IEEE. All rights reserved, including rights for text and data mining and training of artificial intelligence and similar technologies. Personal use is permitted, but republication/redistribution requires IEEE permission. See https://www.ieee.org/publications/rights/index.html for more information.

This article has been accepted for publication in IEEE Antennas and Wireless Propagation Letters. This is the author's version which has not been fully edited and content may change prior to final publication. Citation information: DOI 10.1109/LAWP.2026.3746048

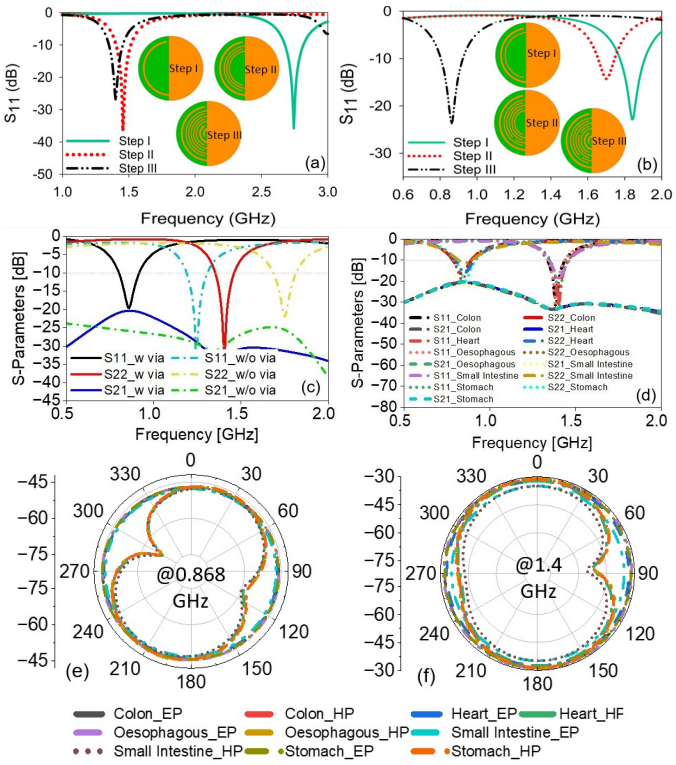


Fig. 3. Antenna evolution and robustness analysis: (a) Port 2 evolution, (b) Port 1 evolution, (c) effect of the via on simulated S-parameters, (d) simulated S-parameters at different in-body locations, and simulated radiation patterns at (e) 0.868 GHz and (f) 1.41 GHz.

0.868 and 1.41 GHz while maintaining low inter-port coupling, confirming its role in resonance control and isolation enhancement. The robustness of the antenna was further examined in five representative in-body environments, namely the colon, heart, oesophagus, small intestine, and stomach. As shown in Fig. 3(d), the two resonant channels and S_{21} isolation remain stable across all phantoms, with only minor shifts caused by variations in tissue loading. Moreover, the radiation patterns at 0.868 and 1.41 GHz in Figs. 3(e) and 3(f), respectively, retain similar characteristics for all investigated locations, demonstrating stable radiation behavior and reliable dual-port operation under variable in-body conditions.

III. Performance Evaluation and Experimental Validation

The performance of the proposed self-duplexing antenna was investigated through full-wave simulations using ANSYS HFSS and CST Studio, followed by experimental validation with a calibrated vector network analyzer (VNA). Fig. 4(a) presents the fabricated prototype, capsule integration, VNA measurement arrangement, and radiation-pattern setup, while the simulated and measured S-parameters are presented separately in Figs. 4(b) and 4(c), respectively. For practical evaluation, the antenna was incorporated into the capsule device and characterized in tissue-representative media to reproduce the highly lossy electromagnetic environment encountered during wireless capsule endoscopy.

For measurement, the capsule was centered and immersed approximately 50 mm in a 0.9% NaCl saline phantom contained in a $200 \times 200 \times 200$ mm^3 nonconductive vessel. The medium properties were approximately $\varepsilon_r = 78.0$, $\sigma = 1.50$ S/m at 0.868 GHz and $\varepsilon_r = 76.0$, $\sigma = 1.85$ S/m at 1.41 GHz. A SOLT-calibrated VNA was used with the reference plane at the coaxial-feed interfaces. The simulated responses exhibit two distinct operating channels centered at 0.868 and 1.41 GHz. At 0.868 GHz, the simulated -10-dB impedance bandwidth extends from 0.80 to 0.92 GHz (120 MHz), whereas the measured response covers approximately 0.79–0.94 GHz (150 MHz). Similarly, the 1.41-GHz channel provides a simulated bandwidth of 1.35–1.46 GHz (110 MHz), which broadens slightly to approximately 1.34–1.48 GHz (140 MHz) in measurement. Thus, both measured operating bands fully encompass their corresponding simulated bandwidths and preserve the intended dual-frequency response.

Figs. 4(d) and 4(e) present the simulated and measured radiation patterns at 0.868 and 1.41 GHz, respectively, in the principal E- and H-planes. Nearly omnidirectional radiation is observed at both frequencies, which is desirable for WCE systems where the capsule orientation varies during gastrointestinal transit. The simulated peak realized gains are -38 and -34.9 dBi at 0.868 and 1.41 GHz, respectively, while the corresponding measured values are approximately -39 and -36 dBi. The realized gain was obtained by comparison with a calibrated broadband reference horn at an approximately 1-m separation in the RF chamber, with the capsule maintained in the same phantom configuration and cable/system losses accounted for through calibration. The small gain reduction in measurement is mainly attributed to fabrication tolerances, capsule integration, and additional losses and dielectric differences in the saline phantom. Overall, the measured patterns closely follow the simulated trends, confirming stable radiation performance under representative in-body conditions.

The transmission coefficient remains substantially below the reflection responses around both resonances, demonstrating weak mutual

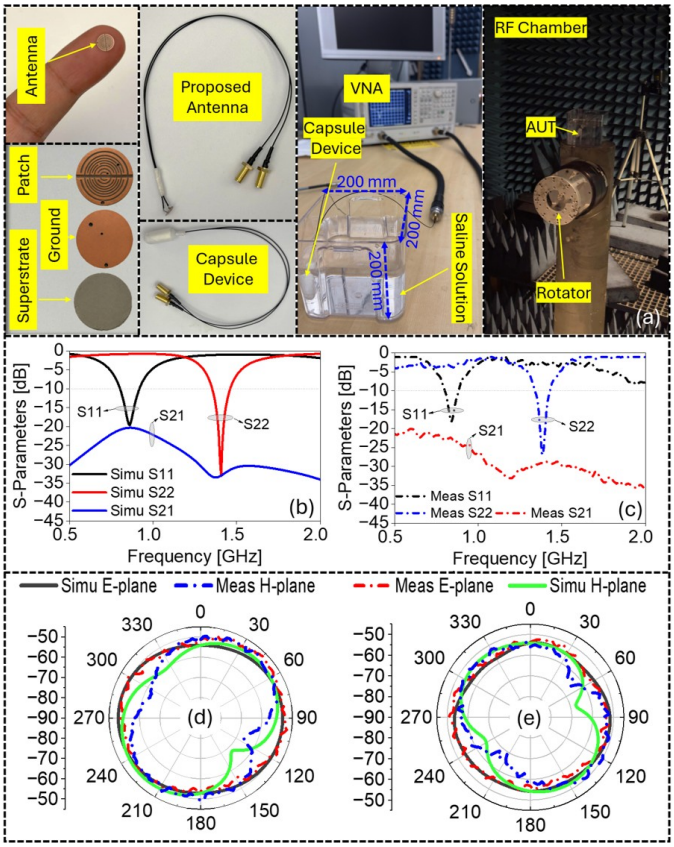


Fig. 4. Experimental validation: (a) fabricated antenna, capsule integration, S-parameter and radiation-measurement setups; (b) simulated and (c) measured S-parameters; simulated and measured radiation patterns at (d) 0.868 GHz and (e) 1.41 GHz.

Authorized licensed use limited to: Auckland University of Technology. Downloaded on November 09,2026 at 22:06:40 UTC from IEEE Xplore. Restrictions apply.
© 2026 IEEE. All rights reserved, including rights for text and data mining and training of artificial intelligence and similar technologies. Personal use is permitted, but republication/redistribution requires IEEE permission. See https://www.ieee.org/publications/rights/index.html for more information.

This article has been accepted for publication in IEEE Antennas and Wireless Propagation Letters. This is the author's version which has not been fully edited and content may change prior to final publication. Citation information: DOI 10.1109/LAWP.2026.3746048

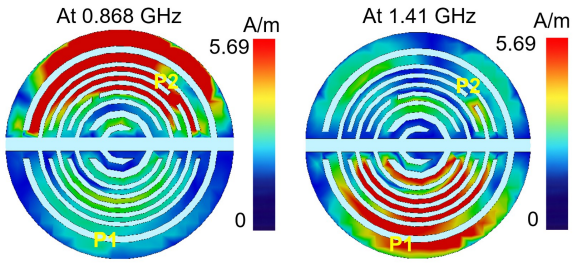


Fig. 5. Simulated surface-current distributions showing frequency-selective current confinement at 0.868 GHz and 1.41 GHz.

coupling and effective frequency isolation between the two ports. This behavior confirms that excitation of one channel has limited influence on the other, which is essential for the intended self-duplexing operation. Overall, the measured S-parameters follow the simulated trends with only moderate variations in resonance depth and bandwidth. These differences are primarily attributed to fabrication and assembly tolerances, coaxial-feed effects, and inevitable variations between the dielectric properties of the experimental media and those assumed in the numerical tissue models. Nevertheless, the measured results preserve both operating bands and provide approximately 22 and 35 dB inter-port isolation at 0.868 and 1.41 GHz, respectively, validating the antenna-level frequency-isolated dual-port operation.

Fig. 5 illustrates the simulated surface-current distributions and the physical origin of the inter-port isolation. At 0.868 GHz, the dominant current follows the loaded resonant path associated with Port 2, while only weak current is induced on the Port 1 radiator. Conversely, at 1.41 GHz, the current is primarily confined to the Port 1 resonant path, with limited excitation of the Port 2 section. This frequency-selective current confinement minimizes modal overlap and power transfer between the two feeds. Together with the continuous ground return path and optimized radiator separation, the weak excitation of the inactive radiator explains the measured isolation of approximately 22 and 35 dB at 0.868 and 1.41 GHz, respectively, thereby supporting antenna-level self-duplexing operation.

Fig. 6 presents the peak spatial-average SAR (spSAR) distributions at 0.868 and 1.41 GHz for 1-g and 10-g tissue masses. The antenna was evaluated in the heterogeneous human-body model using a reference input power of 1 W. The corresponding 1-g/10-g peak SAR values are 456/74.8 W/kg at 0.868 GHz and 328/99.4 W/kg at 1.41 GHz.

Since SAR scales linearly with the accepted input power, the SAR at an arbitrary power P_{in} can be expressed as

$$\mathrm{SAR}(P_{\mathrm{in}}) = \mathrm{SAR}_{1\mathrm{W}} \frac{P_{\mathrm{in}}}{1\ \mathrm{W}}, \tag{1}$$

and the maximum allowable input power (MAP) is obtained from

$$P_{\mathrm{MAP}} = \frac{\mathrm{SAR}_{\mathrm{lim}}}{\mathrm{SAR}_{1\mathrm{W}}} \times 1\ \mathrm{W}. \tag{2}$$

According to IEEE C95.1-2019 and ICNIRP guidelines, the local SAR limit for unrestricted/general-public exposure is 2 W/kg averaged over 10 g of tissue. Accordingly, the 10-g SAR values yield

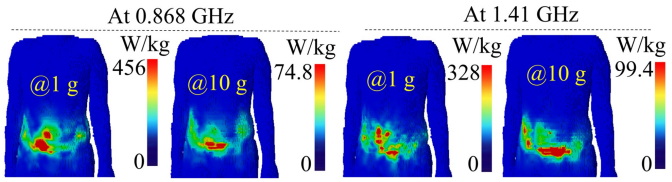


Fig. 6. SAR distributions at 0.868 and 1.41 GHz for 1-g and 10-g tissue masses.

PARAMETERS ADOPTED FOR WCE LINK-BUDGET EVALUATION

Variable	Description	Value
f	Operating frequency (GHz)	0.868, 1.41
G_t	Transmitter antenna gain (dBi)	−38, −34.9
G_r	Receiver antenna gain (dBi)	2.15
P_t	Transmitter power (dBm)	−16
E_b/N_0	Required energy-per-bit to noise ratio (dB)	9.6
R_b	Data rate (Mbps)	50, 78
NF	Receiver noise figure (dB)	3
d_0	Reference distance (m)	0.1
L_{pol}	Polarization/mismatch loss (dB)	10
S	Shadowing margin (dB)	4
n	Path-loss exponent	4

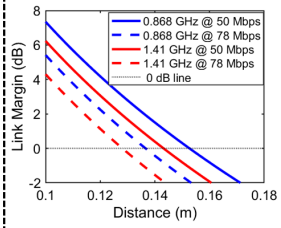


Fig. 7. Adopted link-budget parameters and link-margin characteristics at 0.868 and 1.41 GHz for 50- and 78-Mbps data rates.

maximum allowable input powers of approximately 26.74 mW at 0.868 GHz and 20.12 mW at 1.41 GHz. Thus, operation below these power levels satisfies the adopted 10-g local SAR criterion while providing sufficient margin for low-power WCE telemetry.

To assess the wireless communication capability of the proposed WCE antenna, a theoretical link-budget analysis is performed using the simulated antenna characteristics. The received power at distance d is evaluated using the log-distance path-loss model as

$$P_r(d) = P_t + G_t + G_r - L_{\mathrm{PL}}(d) - L_{\mathrm{pol}} - S, \tag{3}$$

where $L_{\mathrm{PL}}(d) = L_{\mathrm{PL}}(d_0) + 10n\log_{10}(d/d_0)$ and $L_{\mathrm{PL}}(d_0) = 20\log_{10}(4\pi d_0/\lambda)$. Here, d_0 is the reference distance, n is the path-loss exponent, L_{pol} is the polarization/mismatch loss, and S is the shadowing margin. The minimum receiver sensitivity is expressed as

$$P_{r,\min} = -174 + 10\log_{10}(R_b) + NF + \left(\frac{E_b}{N_0}\right)_{\mathrm{req}} \quad (\mathrm{dBm}), \tag{4}$$

where R_b denotes the data rate, NF is the receiver noise figure, and $(E_b/N_0)_{\mathrm{req}}$ is the required energy-per-bit to noise-density ratio. The link margin is then determined from

$$LM(d) = P_r(d) - P_{r,\min}, \tag{5}$$

where a positive value indicates that the received power exceeds the receiver sensitivity.

Fig. 7 presents the calculated link-margin performance at 0.868 and 1.41 GHz for data rates of 50 and 78 Mbps using the parameters in Fig. 7. With $n = 4$, the zero-link-margin distances are approximately 0.153/0.137 m at 0.868 GHz and 0.143/0.128 m at 1.41 GHz for 50/78 Mbps, respectively. Since the capsule/tissue loading is already reflected in the realized gain, an additional 3-dB implementation margin was considered to account for residual orientation, feed, and receiver-placement uncertainties. Under this pessimistic condition, the corresponding ranges reduce to approximately 0.128/0.115 m and 0.120/0.108 m, respectively, confirming the short-range nature of the proposed WCE telemetry link.

IV. CONCLUSION

This letter presents a compact dual-port self-duplexing antenna for wireless capsule endoscopy (WCE). With a volume of only 5.11 mm^3, the antenna provides two independently operating frequency-isolated ports at 0.868 and 1.41 GHz, supporting self-duplexing WCE telemetry without an external duplexing network. The design achieves approximately 22 and 35 dB inter-port isolation, with realized gains of −38 and −34.9 dBi. The 10-g SAR analysis yields maximum permissible input powers of 26.74 and 20.12 mW. The link-budget analysis indicates 50-Mbps communication ranges of approximately 0.153 and 0.143 m at 0.868 and 1.41 GHz, respectively. Experimental results verify the dual-band response and confirm practical antenna-level dual-port operation under representative WCE conditions. Overall, the proposed antenna offers a compact and highly isolated solution for WCE telemetry.

Authorized licensed use limited to: Auckland University of Technology. Downloaded on November 09,2026 at 22:06:40 UTC from IEEE Xplore. Restrictions apply.
© 2026 IEEE. All rights reserved, including rights for text and data mining and training of artificial intelligence and similar technologies. Personal use is permitted, but republication/redistribution requires IEEE permission. See https://www.ieee.org/publications/rights/index.html for more information.

This article has been accepted for publication in IEEE Antennas and Wireless Propagation Letters. This is the author's version which has not been fully edited and content may change prior to final publication. Citation information: DOI 10.1109/LAWP.2026.3746048

REFERENCES

[1] A. Iqbal, S. H. Kiani, M. Al-Hasan, I. Ben Mabrouk, and T. A. Denidni, "A compact dual-band implantable MIMO antenna for wireless capsule endoscopy," *IEEE Trans. Antennas Propag.*, vol. 72, no. 10, pp. 7515–7524, Oct. 2024, doi: 10.1109/TAP.2024.3454434.

[2] S. Ahmad, A. Iqbal, and T. A. Denidni, "Compact and highly-isolated quadruplexing antenna for scalp-implantable IoT devices," *IEEE Internet Things J.*, early access, 2026, doi: 10.1109/JIOT.2026.3694946.

[3] S. H. Kiani *et al.*, "A compact multichannel implantable antenna for high-speed telemetry," *IEEE Trans. Antennas Propag.*, vol. 73, no. 8, pp. 5209–5216, Aug. 2025, doi: 10.1109/TAP.2025.3564738.

[4] A. Alshammari *et al.*, "Ultraminiaturized dual-band implantable antenna for wireless capsule endoscopy," *IEEE Sensors J.*, vol. 24, no. 9, pp. 15210–15218, 2024.

[5] S. M. A. Shah *et al.*, "Four-port triple-band implantable MIMO antenna for reliable data telemetry in wireless capsule endoscopy and deep tissue applications," *IEEE Trans. Antennas Propag.*, vol. 72, no. 8, pp. 6229–6241, Aug. 2024.

[6] S. M. Un Noor *et al.*, "High data-rate Hilbert-curved-shaped MIMO antenna with improved bandwidth and circular polarization for wireless capsule endoscopy," *IEEE Access*, vol. 13, pp. 2876–2889, 2025.

[7] X. Hu *et al.*, "Biomedical applications and challenges of in-body implantable antenna for implantable medical devices: A review," *AEU-Int. J. Electron. Commun.*, vol. 174, Art. no. 155053, 2024.

[8] N. Abbas, A. Basir, A. Iqbal, M. Yousaf, A. Akram, and H. Yoo, "Ultra-miniaturized antenna for deeply implanted biomedical devices," *IEEE Access*, vol. 10, pp. 54563–54571, 2022.

[9] O. F. Celik, Y. E. Yamac, and S. C. Basaran, "Compact multi-band implantable antenna designs for versatile in-body applications," *AEU-Int. J. Electron. Commun.*, vol. 150, Art. no. 154204, Jun. 2022.

[10] I. A. Shah, M. Zada, and H. Yoo, "Design and analysis of a compact-sized multiband spiral-shaped implantable antenna for scalp implantable and leadless pacemaker systems," *IEEE Trans. Antennas Propag.*, vol. 67, no. 6, pp. 4230–4234, Jun. 2019.

[11] A. Basir, M. Zada, Y. Cho, and H. Yoo, "A dual-circular-polarized endoscopic antenna with wideband characteristics and wireless biotelemetric link characterization," *IEEE Trans. Antennas Propag.*, vol. 68, no. 10, pp. 6953–6963, Oct. 2020.

[12] M. Zada and H. Yoo, "Miniaturized dual-band antennas for intraoral tongue drive system in the ISM bands 433 MHz and 915 MHz: Design, safety, and link budget considerations," *IEEE Trans. Antennas Propag.*, vol. 67, no. 9, pp. 5843–5852, Sep. 2019.

[13] A. Iqbal, M. Al-Hasan, I. B. Mabrouk, and T. A. Denidni, "Simultaneous transmit and receive self-duplexing antenna for head implants," *IEEE Trans. Antennas Propag.*, vol. 71, no. 11, pp. 8592–8601, Nov. 2023.

[14] A. Iqbal, M. Al-Hasan, I. B. Mabrouk, and T. A. Denidni, "Wireless powering and telemetry of deep-body ingestible bioelectronic capsule," *IEEE Trans. Antennas Propag.*, vol. 70, no. 10, pp. 9819–9830, Oct. 2022.

[15] A. Iqbal, M. Al-Hasan, I. B. Mabrouk, A. Basir, M. Nedil, and H. Yoo, "Biotelemetry and wireless powering of biomedical implants using a rectifier integrated self-diplexing implantable antenna," *IEEE Trans. Microw. Theory Techn.*, vol. 69, no. 7, pp. 3438–3451, Jul. 2021.

[16] A. Alshammari, A. Basir, M. Zada, S. A. A. Shah, A. Iqbal, and I. Ben Mabrouk, "Miniaturized duplex implantable antenna for wireless data communication and power transfer," *IEEE Open J. Antennas Propag.*, vol. 6, pp. 2062–2073, Dec. 2025, doi: 10.1109/OJAP.2025.3619468.

[17] A. Iqbal, M. Al-Hasan, I. B. Mabrouk, and T. A. Denidni, "Broadband duplex antenna for implantable medical devices," *IEEE Trans. Antennas Propag.*, early access, 2026.

[18] A. Alshammari *et al.*, "Compact in-band full-duplex antenna for deeply implantable biomedical IoT applications," *IEEE Internet Things J.*, early access, 2026.

[19] S. M. Un Noor *et al.*, "A highly miniaturized circularly polarized self-duplexing implantable antenna with enhanced performance for wireless capsule endoscopy applications," *Sci. Rep.*, vol. 15, no. 1, Art. no. 35470, 2025.

[20] N. Vasugi and M. Karthikeyan, "A conformal triple-band capsule antenna based on hybrid T-shaped-rhombus resonator," *IEEE Antennas Wireless Propag. Lett.*, vol. 25, no. 7, pp. 2683–2687, Jul. 2026, doi: 10.1109/LAWP.2026.3688177.

[21] H. Liu *et al.*, "Novel multiband antenna design and performance evaluation for wireless electronic capsule systems," *IEEE J. Electromagn., RF Microw. Med. Biol.*, vol. 8, no. 4, pp. 332–343, Dec. 2024, doi: 10.1109/JERM.2024.3401572.

[22] S. Ahlawat *et al.*, "Design and performance measurement of implantable differential integrated antenna for wireless biomedical instrumentation applications," *IEEE Trans. Instrum. Meas.*, vol. 71, Art. no. 5502110, pp. 1–10, 2022, doi: 10.1109/TIM.2022.3185622.

[23] Y. Fan *et al.*, "Novel coated differentially fed dual-band fractal antenna for implantable medical devices," *IET Microw., Antennas Propag.*, vol. 14, no. 3, pp. 199–208, 2020, doi: 10.1049/iet-map.2018.6171.

Authorized licensed use limited to: Auckland University of Technology. Downloaded on November 09,2026 at 22:06:40 UTC from IEEE Xplore. Restrictions apply.
© 2026 IEEE. All rights reserved, including rights for text and data mining and training of artificial intelligence and similar technologies. Personal use is permitted,
but republication/redistribution requires IEEE permission. See https://www.ieee.org/publications/rights/index.html for more information.